

Signature of a Pairing Transition in the Heat Capacity of Finite Nuclei

S. Liu and Y. Alhassid

*Center for Theoretical Physics, Sloane Physics Laboratory, Yale University, New Haven,
Connecticut 06520, U.S.A.*

(June 24, 2018)

Abstract

The heat capacity of iron isotopes is calculated within the interacting shell model using the complete $(pf + 0g_{9/2})$ -shell. We identify a signature of the pairing transition in the heat capacity that is correlated with the suppression of the number of spin-zero neutron pairs as the temperature increases. Our results are obtained by a novel method that significantly reduces the statistical errors in the heat capacity calculated by the shell model Monte Carlo approach. The Monte Carlo results are compared with finite-temperature Fermi gas and BCS calculations.

arXiv:nucl-th/0009006v1 5 Sep 2000

Pairing effects in finite nuclei are well known; examples include the energy gap in the spectra of even-even nuclei and an odd-even effect observed in nuclear masses. However, less is known about the thermal signatures of the pairing interaction in nuclei. In a macroscopic conductor, pairing leads to a phase transition from a normal metal to a superconductor below a certain critical temperature, and in the BCS theory [1] the heat capacity is characterized by a finite discontinuity at the transition temperature. As the linear dimension of the system decreases below the pair coherence length, fluctuations in the order parameter become important and lead to a smooth transition. The effects of both static fluctuations [2,3] and small quantal fluctuations [4] have been explored in studies of small metallic grains. A pronounced peak in the heat capacity is observed for a large number of electrons, but for less than ~ 100 electrons the peak in the heat capacity all but disappears. In the nucleus, the pair coherence length is always much larger than the nuclear radius, and large fluctuations are expected to suppress any singularity in the heat capacity. An interesting question is whether any signature of the pairing transition still exists in the heat capacity of the nucleus despite the large fluctuations. When only static and small-amplitude quantal fluctuations are taken into account, a shallow ‘kink’ could still be seen in the heat capacity of an even-even nucleus [5]. This calculation, however, was limited to a schematic pairing model. Canonical heat capacities were recently extracted from level density measurements in rare-earth nuclei [6] and were found to have an *S*-shape that is interpreted to represent the suppression of pairing correlations with increasing temperature.

The calculation of the heat capacity of the finite interacting nuclear system beyond the mean-field and static-path approximations is a difficult problem. Correlation effects due to residual interactions can be accounted for in the framework of the interacting nuclear shell model. However, at finite temperature a large number of excited states contribute to the heat capacity and very large model spaces are necessary to obtain reliable results. The shell model Monte Carlo (SMMC) method [7,8] enables zero- and finite-temperature calculations in large spaces. In particular, the thermal energy $E(T)$ can be computed versus temperature T and the heat capacity can be obtained by taking a numerical derivative $C = dE/dT$. However,

the finite statistical errors in $E(T)$ lead to large statistical errors in the heat capacity at low temperatures (even for good-sign interactions). Such large errors occur already around the pairing transition temperature and thus no definite signatures of the pairing transition could be identified. Furthermore, the large errors often lead to spurious structure in the calculated heat capacity. Presumably, a more accurate heat capacity can be obtained by a direct calculation of the variance of the Hamiltonian, but in SMMC such a calculation is impractical since it involves a four-body operator. The variance of the Hamiltonian has been calculated using a different Monte Carlo algorithm [9], but that method is presently limited to a schematic pairing interaction. Here we report a novel method for calculating the heat capacity within SMMC that takes into account correlated errors and leads to much smaller statistical errors. Using this method we are able to identify a signature of the pairing transition in *realistic* calculations of the heat capacity of finite nuclei. The signature is well correlated with the suppression in the number of spin-zero pairs across the transition temperature.

The Monte Carlo approach is based on the Hubbard-Stratonovich (HS) representation of the many-body imaginary-time propagator, $e^{-\beta H} = \int D[\sigma] G_\sigma U_\sigma$, where β is the inverse temperature, G_σ is a Gaussian weight and U_σ is a one-body propagator that describes non-interacting nucleons moving in fluctuating time-dependent auxiliary fields σ . The canonical thermal expectation value of an observable O can be written as $\langle O \rangle = \int D[\sigma] G_\sigma \text{Tr}(OU_\sigma) / \int D[\sigma] G_\sigma \text{Tr} U_\sigma$, where Tr denotes a canonical trace for N neutrons and Z protons. We can rewrite

$$\langle O \rangle = \frac{\langle [\text{Tr}(OU_\sigma) / \text{Tr} U_\sigma] \Phi_\sigma \rangle_W}{\langle \Phi_\sigma \rangle_W}, \quad (1)$$

where $\Phi_\sigma = \text{Tr} U_\sigma / |\text{Tr} U_\sigma|$ is the Monte Carlo sign, and we have used the notation $\langle X_\sigma \rangle_W \equiv \int D[\sigma] W(\sigma) X_\sigma / \int D[\sigma] W(\sigma)$ with $W(\sigma) \equiv G_\sigma |\text{Tr} U_\sigma|$. In SMMC we divide the imaginary-time interval $(0, \beta)$ into N_t time slices of length $\Delta\beta = \beta/N_t$, and sample the fields $\sigma(\tau_n)$ fields at all N_t time slices $\tau_n = n\Delta\beta$ according to the positive-definite weight function $W(\sigma)$. Each quantity $\langle X_\sigma \rangle_W$ in Eq. (1) is then estimated as an arithmetic average over the chosen

samples.

In particular the thermal energy can be calculated as a thermal average of the Hamiltonian H . The heat capacity $C = -\beta^2 \partial E / \partial \beta$ is then calculated by estimating the derivative as a finite difference

$$C = -\beta^2 \frac{E(\beta + \delta\beta) - E(\beta - \delta\beta)}{2\delta\beta} + O(\delta\beta)^2. \quad (2)$$

At low temperatures, $E(\beta)$ decreases slowly with β and even small errors in $E(\beta)$ lead to relatively large statistical errors in C . Conventionally, the calculation of $E(\beta)$ for each β is done by a new Monte Carlo sampling of the σ fields and consequently the energies $E(\beta - \delta\beta)$ and $E(\beta + \delta\beta)$ in (2) are uncorrelated. However, if the calculation of both $E(\beta \pm \delta\beta)$ can be done using a common set of sampling fields, the correlated errors of C are expected to be smaller.

The energies $E(\beta \pm \delta\beta)$ are calculated from

$$E(\beta \pm \delta\beta) = \frac{\int D[\sigma^\pm] G_{\sigma^\pm}(\beta \pm \delta\beta) \text{Tr}[HU_{\sigma^\pm}(\beta \pm \delta\beta)]}{\int D[\sigma^\pm] G_{\sigma^\pm}(\beta \pm \delta\beta) \text{Tr}U_{\sigma^\pm}(\beta \pm \delta\beta)}, \quad (3)$$

where the corresponding σ fields are denoted by σ^\pm . To have the same number of time slices N_t in the discretized version of (3) as in the original HS representation of $E(\beta)$, we define modified time slices $\Delta\beta_\pm$ by $N_t \Delta\beta_\pm = \beta \pm \delta\beta$. We next change integration variables in (3) from σ^\pm to σ according to $\sigma^\pm = (\Delta\beta / \Delta\beta_\pm)^{1/2} \sigma$, so that the Gaussian weight is left unchanged $G_{\sigma^\pm}(\beta \pm \delta\beta) \equiv \exp\left[-\sum_{\alpha n} \frac{1}{2} |v_\alpha| (\sigma_\alpha^\pm(\tau_n))^2 \Delta\beta_\pm\right] = \exp\left[-\sum_{\alpha n} \frac{1}{2} |v_\alpha| (\sigma_\alpha(\tau_n))^2 \Delta\beta\right] = G_\sigma(\beta)$ (v_α are the interaction ‘eigenvalues’, obtained by writing the interaction in a quadratic form $\sum_\alpha v_\alpha \hat{\rho}_\alpha^2 / 2$, where $\hat{\rho}_\alpha$ are one-body densities). Rewriting (3) using the measure $D[\sigma]$ (the Jacobian resulting from the change in integration variables is constant and canceled between the numerator and denominator), we find

$$E(\beta \pm \delta\beta) = \frac{\left\langle \frac{\text{Tr}HU_{\sigma^\pm(\beta \pm \delta\beta)}}{\text{Tr}U_{\sigma^\pm(\beta \pm \delta\beta)}} \frac{\text{Tr}U_{\sigma^\pm(\beta \pm \delta\beta)}}{\text{Tr}U_{\sigma(\beta)}} \Phi_\sigma \right\rangle_W}{\left\langle \frac{\text{Tr}U_{\sigma^\pm(\beta \pm \delta\beta)}}{\text{Tr}U_{\sigma(\beta)}} \Phi_\sigma \right\rangle_W} \equiv \frac{H_\pm}{Z_\pm}. \quad (4)$$

The heat capacity in (2) is calculated from $C = -\beta^2 (2\delta\beta)^{-1} (H_+ / Z_+ - H_- / Z_-)$. Since the same set of fields σ is used in the calculation of both $E(\beta \pm \delta\beta)$, we expect strong correlations

among the quantities H_{\pm} and Z_{\pm} , which would lead to a smaller error for C . The covariances among H_{\pm} and Z_{\pm} as well as their variances can be calculated in the Monte Carlo and used to estimate the correlated error of the heat capacity.

We have calculated the heat capacity for the iron isotopes $^{52-62}\text{Fe}$ using the complete $(pf + 0g_{9/2})$ -shell and the good-sign interaction of Ref. [10]. Fig. 1 demonstrates the significant improvement in the statistical Monte Carlo errors. On the left panel of this figure we show the heat capacity of ^{54}Fe calculated in the conventional method, while the right panel shows the results from the new method. The statistical errors for $T \sim 0.5 - 1$ MeV are reduced by almost an order of magnitude. The results obtained in the conventional calculation seem to indicate a shallow peak in the heat capacity around $T \sim 1.25$ MeV, but the calculation using the improved method shows no such structure.

The heat capacities of four iron isotopes $^{55-58}\text{Fe}$, calculated with the new method, are shown in the top panel of Fig. 2. The heat capacities of the two even-mass iron isotopes (^{56}Fe and ^{58}Fe) show a different behavior around $T \sim 0.7 - 0.8$ MeV as compared with the two odd-mass isotopes (^{55}Fe and ^{57}Fe). While the heat capacity of the odd-mass isotopes increases smoothly as a function of temperature, the heat capacity of the even-mass isotopes is enhanced for $T \sim 0.6 - 1$ MeV, increasing sharply and then leveling off, displaying a ‘shoulder.’ This ‘shoulder’ is more pronounced for the isotope with more neutrons (^{58}Fe). To correlate this behavior of the heat capacity with a pairing transition, we calculated the number of $J = 0$ nucleon pairs in these nuclei. A $J = 0$ pair operator is defined as usual by

$$\Delta^{\dagger} = \sum_{a, m_a > 0} \frac{(-1)^{j_a - m_a}}{\sqrt{j_a + 1/2}} a_{j_a m_a}^{\dagger} a_{j_a - m_a}^{\dagger}, \quad (5)$$

where j_a is the spin and m_a is the spin projection of a single-particle orbit a . Pair-creation operators of the form (5) can be defined for protons (Δ_{pp}^{\dagger}), neutrons (Δ_{nn}^{\dagger}), and proton-neutrons (Δ_{pn}^{\dagger}). The average number $\langle \Delta^{\dagger} \Delta \rangle$ of $J = 0$ pairs (of each type) can be calculated exactly in SMMC as a function of temperature. The bottom panel of Fig. 2 shows the number of neutron pairs $\langle \Delta_{nn}^{\dagger} \Delta_{nn} \rangle$ for $^{55-58}\text{Fe}$. At low temperature the number of neutron pairs for isotopes with an even number of neutrons is significantly larger than that for

isotopes with an odd number of neutrons. Furthermore, for the even-mass isotopes we observe a rapid suppression of the number of neutron pairs that correlates with the ‘shoulder’ observed in the heat capacity. The different qualitative behavior in the number of neutron pairs versus temperature between odd- and even-mass iron isotopes provides a clue to the difference in their heat capacities. A transition from a pair-correlated ground state to a normal state at higher temperatures requires additional energy for breaking of neutron pairs, hence the steeper increase observed in the heat capacity of the even-mass iron isotopes. Once the pairs are broken, less energy is required to increase the temperature, and the heat capacity shows only a moderate increase.

It is instructive to compare the SMMC heat capacity with a Fermi gas and BCS calculations. The heat capacity can be calculated from the entropy using the relation $C = T\partial S/\partial T$. The entropy S of uncorrelated fermions is given by

$$S(T) = - \sum_a [f_a \ln f_a + (1 - f_a) \ln(1 - f_a)] , \quad (6)$$

with f_a being the finite-temperature occupation numbers of the single-particle orbits a . Above the pairing transition-temperature T_c , f_a are just the Fermi-Dirac occupancies $f_a = [1 + e^{\beta(\epsilon_a - \mu)}]^{-1}$, where μ is the chemical potential determined from the total number of particles and ϵ_a are the single-particle energies. Below T_c , it is necessary to take into account the BCS solution which has lower free energy. Since condensed pairs do not contribute to the entropy, the latter is still given by (6) but f_a are now the quasi-particle occupancies [1],

$$f_a = \frac{1}{1 + e^{\beta E_a}} . \quad (7)$$

$E_a = \sqrt{(\epsilon_a - \mu)^2 + \Delta^2}$ are the quasi-particle energies, where the gap $\Delta(T)$ and the chemical potential $\mu(T)$ are determined from the finite-temperature BCS equations. In practice, we treat protons and neutrons separately.

We applied the Fermi gas and BCS approximations to estimate the heat capacities of the iron isotopes. To take into account effects of a quadrupole-quadrupole interaction, we used an axially deformed Woods-Saxon potential to extract the single-particle spectrum ϵ_a [11].

A deformation parameter δ for the even iron isotopes can be extracted from experimental $B(E2)$ values. However, since $B(E2)$ values are not available for all of these isotopes, we used an alternate procedure. The excitation energy $E_x(2_1^+)$ of the first excited 2^+ state in even-even nuclei can be extracted in SMMC by calculating $\langle J^2 \rangle_\beta$ at low temperatures and using a two-state model (the 0^+ ground state and the first excited 2^+ state) where $\langle J^2 \rangle_\beta \approx 6/(1 + e^{\beta E_x(2_1^+)})/5$ [12]. The excitation energy of the 2_1^+ state is then used in the empirical formula of Bohr and Mottelson [13] $\tau_\gamma = (5.94 \pm 2.43) \times 10^{14} E_x^{-4}(2_1^+) Z^{-2} A^{1/3}$ to estimate the mean γ -ray lifetime τ_γ and the corresponding $B(E2)$. The deformation parameter δ is then estimated from $B(E2) = [(3/4\pi) Z e r_0^2 A^{2/3} \delta]^2 / 5$. We find (using $r_0 = 1.27$ fm) $\delta = 0.225, 0.215, 0.244, 0.222, 0.230$, and 0.220 for the even iron isotopes $^{52}\text{Fe} - ^{62}\text{Fe}$, respectively. For the odd-mass iron isotopes we adapt the deformations in Ref. [14]. The zero-temperature pairing gap Δ is extracted from experimental odd-even mass differences and used to determine the pairing strength G (needed for the finite temperature BCS solution).

The top panels of Fig. 3 show the Fermi-gas heat capacity (dotted-dashed lines) for ^{59}Fe (right) and ^{60}Fe (left) in comparison with the SMMC results (symbols). The SMMC heat capacity in the even-mass ^{60}Fe is below the Fermi-gas estimate for $T \lesssim 0.5$ MeV, but is enhanced above the Fermi gas heat capacity in the region $0.5 \lesssim T \lesssim 0.9$ MeV. The line shape of the heat capacity is similar to the S -shape found experimentally in the heat capacity of rare-earth nuclei [6]. We remark that the saturation of the SMMC heat capacity above ~ 1.5 MeV (and eventually its decrease with T) is an artifact of the finite model space. The solid line shown for ^{60}Fe is the result of the BCS calculation. There are two ‘peaks’ in the heat capacity corresponding to separate pairing transitions for neutrons ($T_c^n \approx 0.9$ MeV) and protons ($T_c^p \approx 1.2$ MeV). The finite discontinuities in the BCS heat capacity are shown by the dotted lines. The pairing solution describes well the SMMC results for $T \lesssim 0.6$ MeV. However, the BCS peak in the heat capacity is strongly suppressed around the transition temperature. This is expected in the finite nuclear system because of the strong fluctuations in the vicinity of the pairing transition (not accounted for in the

mean-field approach). Despite the large fluctuations, a ‘shoulder’ still remains around the neutron-pairing transition temperature.

The bottom panels of Fig. 3 show the number of spin-zero pairs versus temperature in SMMC. The number of p - p and n - p pairs are similar in the even and odd-mass iron isotopes. However, the number of n - n pairs at low T differs significantly between the two isotopes. The n - n pair number of ^{60}Fe decreases rapidly as a function of T , while that of ^{59}Fe decreases slowly. The S-shape or shoulder seen in the SMMC heat capacity of ^{60}Fe correlates well with the suppression of neutron pairs.

Fig. 4 shows the complete systematics of the heat capacity for the iron isotopes in the mass range $A = 52 - 62$ for both even-mass (left panel) and odd-mass (right panel). At low temperatures the heat capacity approaches zero, as expected. When T is high, the heat capacity for all isotopes converges to approximately the same value. In the intermediate temperature region ($T \sim 0.7$ MeV), the heat capacity increases with mass due to the increase of the density of states with mass. Pairing leads to an odd-even staggering effect in the mass dependence (see also in Fig. 2) where the heat capacity of an odd-mass nucleus is significantly lower than that of the adjacent even-mass nuclei. For example, the heat capacity of ^{57}Fe is below that of both ^{56}Fe and ^{58}Fe . The heat capacities of the even-mass ^{58}Fe , ^{60}Fe , and ^{62}Fe all display a peak around $T \sim 0.7$ MeV, which becomes more pronounced with an increasing number of neutrons.

In conclusion, we have introduced a new method for calculating the heat capacity in which the statistical errors are strongly reduced. A systematic study in several iron isotopes reveals signatures of the pairing transition in the heat capacity of finite nuclei despite the large fluctuations.

This work was supported in part by the Department of Energy grants No. DE-FG-0291-ER-40608. Computational cycles were provided by the San Diego Supercomputer Center (using NPACI resources), and by the NERSC high performance computing facility at LBL.

REFERENCES

- [1] J. Bardeen, L.N. Cooper and J.R. Schrieffer, Phys. Rev. **108**, 1175 (1957).
- [2] B. Muhlschlegel, D.J. Scalapino and R. Denton, Phys. Rev. B **6**, 1767 (1972).
- [3] B. Lauritzen, P. Arve and G.F. Bertsch, Phys. Rev. Lett. **61**, 2835 (1988).
- [4] B. Lauritzen, A. Anselmino, P.F. Bortignon and R.A. Broglia, Ann. Phys. (N.Y.) **223**, 216 (1993).
- [5] R. Rossignoli, N. Canosa and P. Ring, Phys. Rev. Lett. **80**, 1853 (1998).
- [6] A. Schiller, A. Bjerve, M. Guttormsen, M. Hjorth-Jensen, F. Ingebretsen, E. Melby, S. Messelt, J. Rekstad, S. Siem, S.W. Odegard, arXiv:nucl-ex/9909011.
- [7] G. H. Lang, C. W. Johnson, S. E. Koonin and W. E. Ormand, Phys. Rev. **C48**, 1518 (1993).
- [8] Y. Alhassid, D. J. Dean, S. E. Koonin, G. H. Lang, and W. E. Ormand, Phys. Rev. Lett. **72**, 613 (1994).
- [9] S. Rombouts S, K. Heyde and N. Jachowicz, Phys. Rev. C **58**, 3295 (1998).
- [10] H. Nakada, Y. Alhassid, Phys. Rev. Lett. **79**, 2939 (1997).
- [11] Y. Alhassid, G.F. Bertsch, S. Liu and H. Nakada, Phys. Rev. Lett. **84**, 4313 (2000).
- [12] H. Nakada, Y. Alhassid, Phys. Lett. B **436**, 231 (1998).
- [13] S. Raman *et al.*, Atomic Data and Nuclear Data Tables **42**, 1 (1989).
- [14] P. Möller *et al*, Atomic Data Nucl. Data Tables **59**, 185 (1995), P. Möller, J. R. Nix, and K.-L. Kratz, Atomic Data Nucl. Data Tables **66**, 131 (1997); G. Audi *et al*, Nucl. Phys. **A624**, 1 (1997).

FIGURES

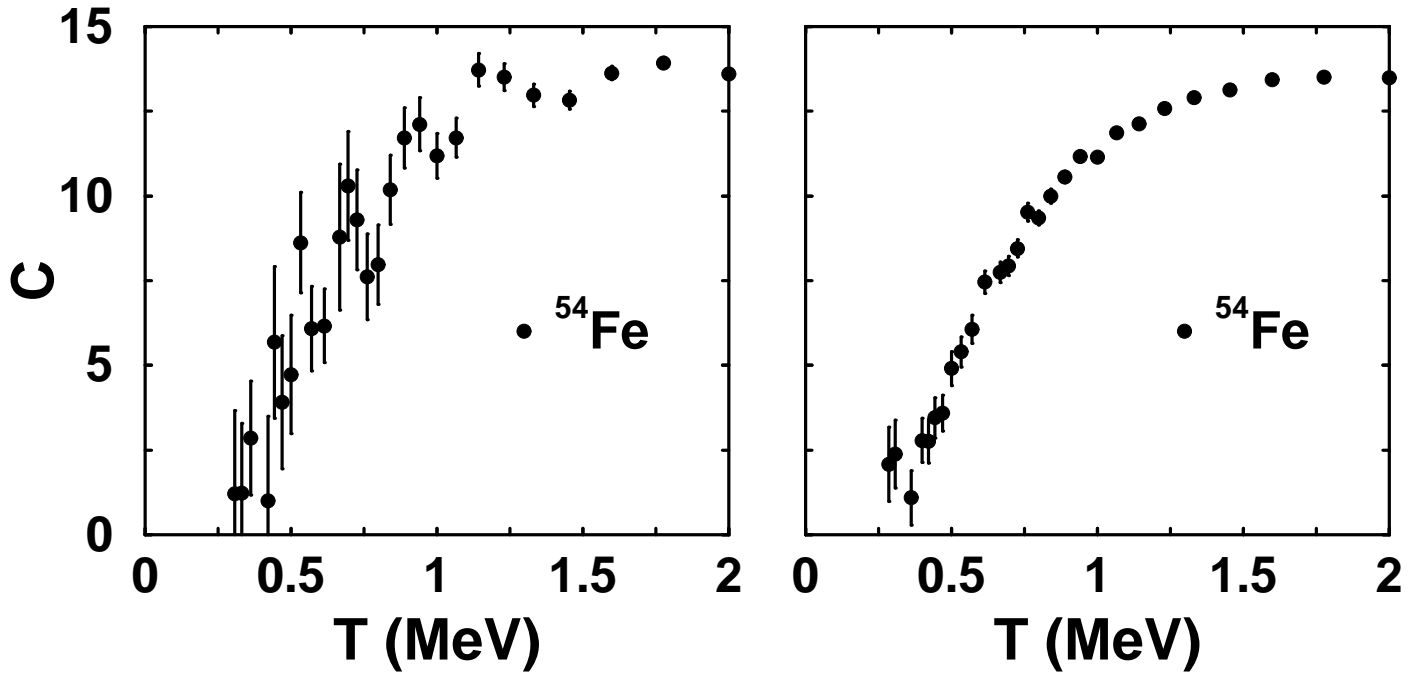


FIG. 1. The SMMC heat capacity of ^{54}Fe . The left panel is the result of conventional SMMC calculations. The right panel is calculated using the improved method (based on the representation (4) where a correlated error can be accounted for).

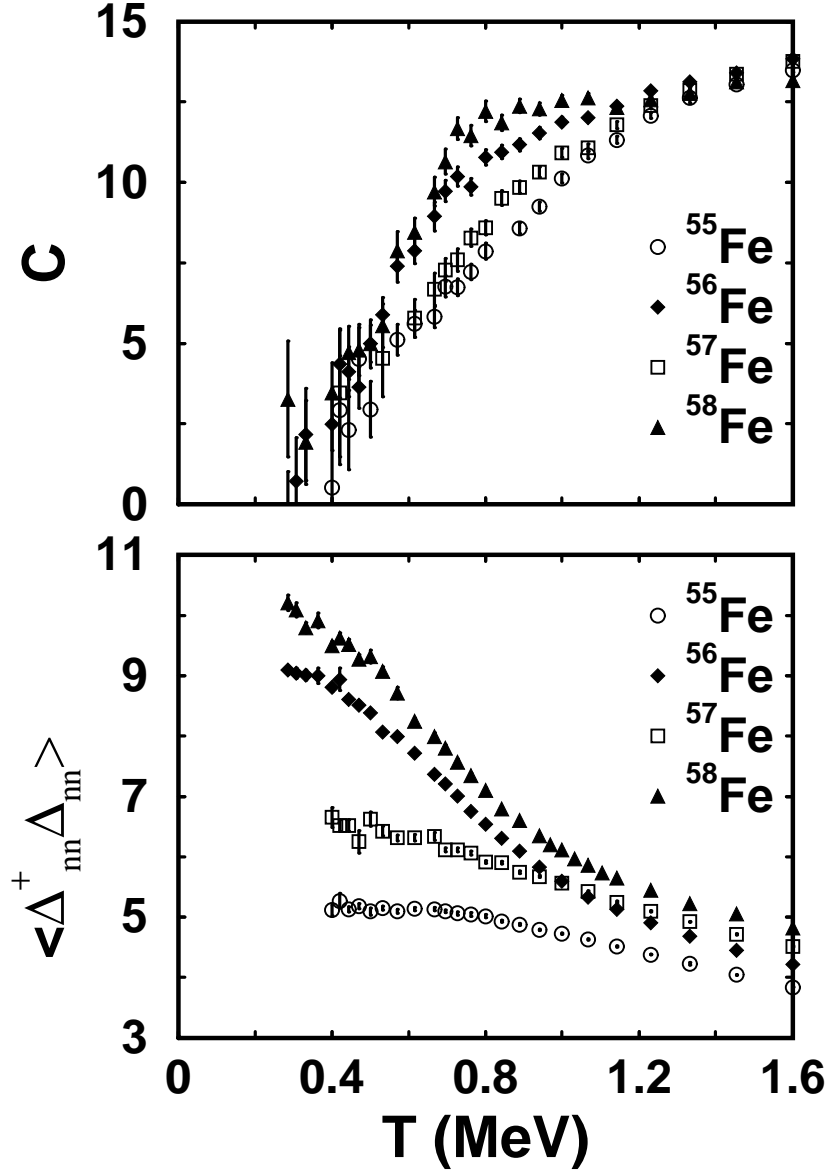


FIG. 2. Top panel: the SMMC heat capacity vs. temperature T for ^{55}Fe (open circles), ^{56}Fe (solid diamonds), ^{57}Fe (open squares), and ^{58}Fe (solid triangles). Bottom panel: the number of $J = 0$ neutron pairs versus temperature for the same nuclei.

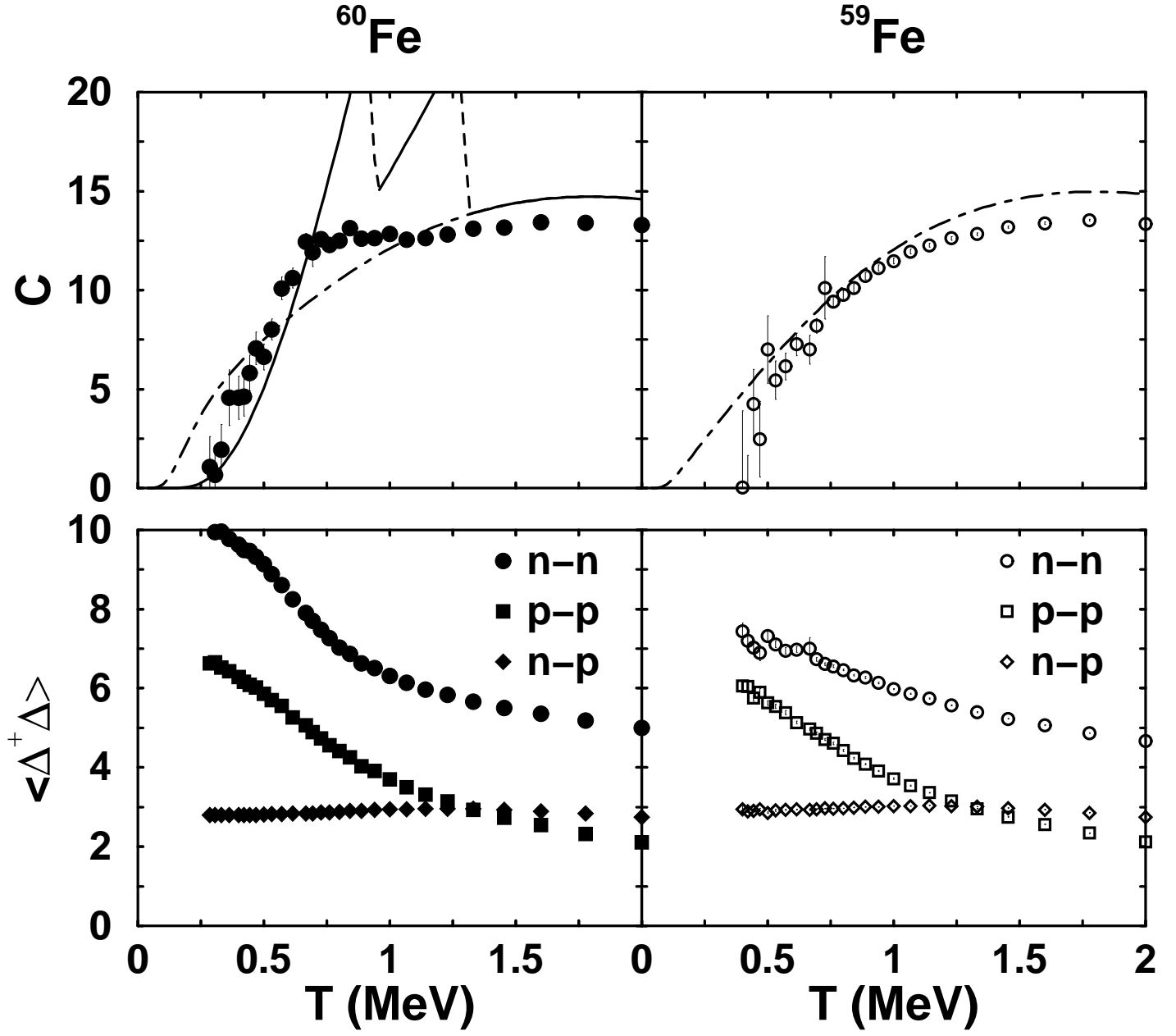


FIG. 3. Top: Heat capacity versus T for ^{60}Fe (left) and ^{59}Fe (right). The Monte Carlo results are shown by symbols. The dotted-dashed lines are the Fermi gas calculations, and the solid line (left panel only) is the BCS result. The discontinuities (dashed lines) correspond to a neutron ($T_c \sim 0.9$ MeV) and proton ($T_c \sim 1.2$ MeV) pairing transition. Above the pairing-transition temperature, the BCS results coincide with the Fermi gas results. Bottom panels: The number of $J=0$ n - n (circles), p - p (squares), and n - p (diamonds) pairs vs. T for ^{60}Fe (left) and ^{59}Fe (right).

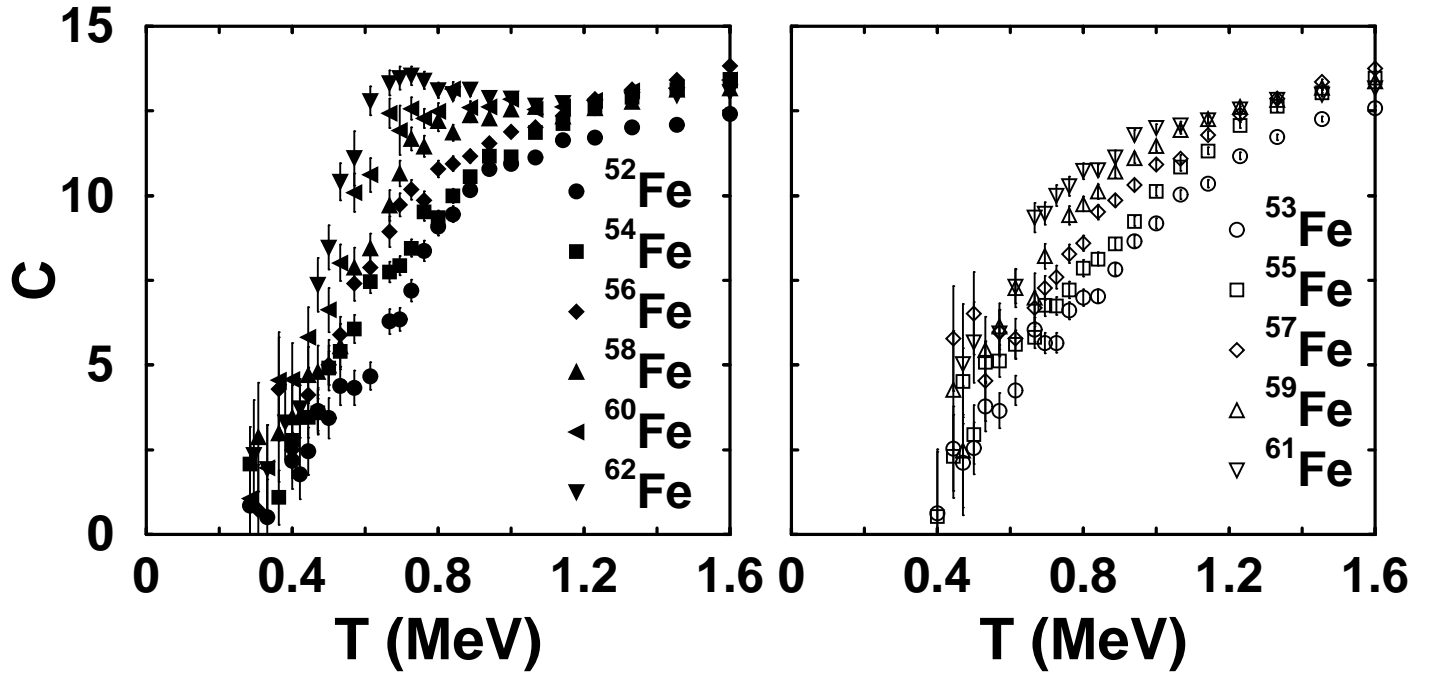


FIG. 4. The heat capacity of even-even (left panel) and odd-even (right panel) iron isotopes.